International Journal of Applied Mathematics
Volume 38 No. 6s, 2025
ISSN: 1311-1728 (printed version); ISSN: 1314-8060 (on-line version)

POWER QUALITY ENHANCEMENT IN PV–PMSG GRIDS USING WHALE OPTIMIZATION-TUNED STATCOM

Ankit Patel [1], Dinesh Singh [2], Kanhaiya Kumar [2]*

[1] Department of Electrical, Electronics and Communication Engineering
Galgotias University
Greater Noida-201310, India
e-mail: apatel30698@gmail.com

[2] Department of Electrical, Electronics and Communication Engineering Galgotias University
Greater Noida-201310, India
e-mail: dineshsingh97@rediffmail.com

[3] Department of Electrical and Electronics Engineering
Galgotias College of Engineering and Technology
Greater Noida-201310, India
e-mail: kkanhaiyakumar@gmail.com

September 26, 2025

Abstract

The increasing penetration of renewable energy sources such as photovoltaic (PV) systems and permanent magnet synchronous generators (PMSGs) in distribution networks has introduced significant power quality challenges. This paper proposes a novel approach for improving the power quality of a grid-connected hybrid renewable system by employing a Static Synchronous Compensator (STATCOM) whose Proportional-Integral (PI) controller parameters are optimally tuned using the Whale Optimization Algorithm (WOA). Three distinct loading conditions — moderate load, heavy load surge, and light load — are considered to evaluate the system's dynamic and steady-state performance. The optimized STATCOM effectively mitigates voltage dips, reduces power oscillations, and improves system transient response. Detailed time-domain simulations demonstrate that the proposed WOA-tuned STATCOM significantly enhances voltage stability, minimizes peak overshoot, improves settling time, and reduces harmonic distortions. Furthermore, the system performance under different loading scenarios confirms the superiority of the WOA-based optimization in stabilizing the hybrid renewable grid interface. The study also outlines directions for future expansion by considering nonlinear and unbalanced load impacts on system dynamics.

Math. Subject Classification:93-10 Mathematical modeling or simulation for problems pertaining to systems and control theory

Received: August 06, 2025

International Journal of Applied Mathematics
Volume 38 No. 6s, 2025
ISSN: 1311-1728 (printed version); ISSN: 1314-8060 (on-line version)

Key Words and Phrases: Power Quality, Whale Optimization Algorithm, PMSG, Distribution System, Renewable energy

1 Introduction

The global transition towards sustainable energy has accelerated the deployment of renewable energy sources (RESs), particularly photovoltaic (PV) systems and wind energy conversion systems (WECSs) using permanent magnet synchronous generators (PMSGs), in modern power networks. These distributed generation (DG) technologies significantly reduce greenhouse gas emissions and fossil fuel dependence [1-3]. However, their stochastic and intermittent characteristics introduce critical operational issues, including voltage instability, frequency deviation, harmonic distortions, and power oscillations, which degrade overall grid reliability and power quality [4-6]. Ensuring stable and high-quality power in RES-integrated distribution networks necessitates advanced control and compensation strategies. Flexible AC Transmission System (FACTS) devices, such as the Static Synchronous Compensator (STATCOM), have been widely adopted due to their superior capability for fast dynamic reactive power compensation, voltage regulation, and harmonic mitigation at the point of common coupling (PCC) [7-9]. Nevertheless, the effectiveness of a STATCOM heavily relies on the performance of its Proportional–Integral (PI) controllers, whose gains must be carefully tuned to handle nonlinear dynamics and fast transients. Conventional manual and heuristic tuning approaches often fail under varying load and fault conditions, leading to inadequate dynamic responses [10-11]. To overcome these limitations, intelligent optimization algorithms have gained prominence in tuning STATCOM controllers in hybrid RES systems. Several metaheuristic techniques, including Particle Swarm Optimization (PSO), Genetic Algorithm (GA), Differential Evolution (DE), and Artificial Bee Colony (ABC), have been explored to enhance voltage stability and harmonic suppression [12-14]. Recently, the Whale Optimization Algorithm (WOA), inspired by the bubble-net hunting behavior of humpback whales, has emerged as a powerful optimizer due to its balance of exploration and exploitation, simplicity, and fast convergence in solving nonlinear control problems [15-17]. WOA has demonstrated promising results in diverse power system applications, including PI/PID tuning, fault ride-through capability improvement, and harmonic reduction in hybrid renewable grids [18-19]. Specifically, its application in optimally tuning STATCOM controllers for PV–PMSG hybrid systems has shown significant improvements in transient performance, settling time, overshoot minimization, and voltage profile regulation under varying load conditions [20]. In this study, a WOA-based PI-STATCOM control strategy is proposed for a grid-connected hybrid PV–PMSG system. The system is evaluated under three representative loading scenarios—moderate, heavy surge, and light load—to examine dynamic and steady-state behaviours. Key performance metrics include voltage stability, harmonic distortion, and transient response. Additionally, the study acknowledges the limitations of uniform load modeling and recommends incorporating nonlinear and unbalanced load profiles in future investigations to provide a more comprehensive validation of controller performance in practical environments.

Received: August 06, 2025

International Journal of Applied Mathematics
Volume 38 No. 6s, 2025
ISSN: 1311-1728 (printed version); ISSN: 1314-8060 (on-line version)

2 System Description

The proposed hybrid renewable energy system integrates both solar photovoltaic (PV) and wind energy sources to ensure a reliable and sustainable power supply to the connected load and grid shown in Figure 1. The PV array is interfaced with a buck-boost DCDC converter to regulate [21-23] the output voltage and enable effective operation under varying irradiance conditions. A Maximum Power Point Tracking (MPPT) system [24-26], typically employing Perturb & Observe (P&O) or Incremental Conductance algorithms, is employed to extract the maximum available power from the PV module. Concurrently, a wind turbine generator feeds power into the system through an uncontrolled rectifier that converts the variable-frequency AC output into DC. This rectified wind energy is also processed through an MPPT unit to optimize energy extraction.

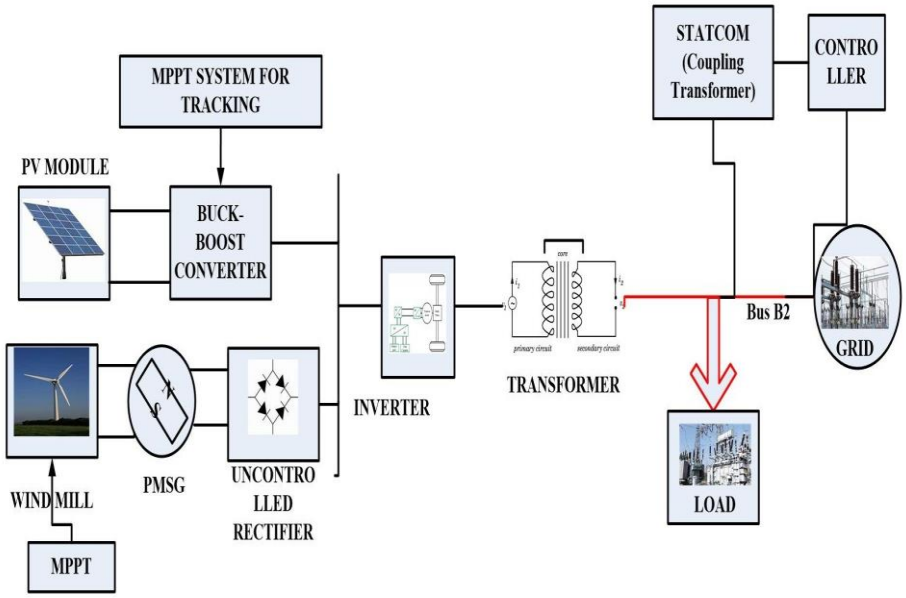

Figure 1: Solar-Wind combination renewable energy equipment coupled to a distributed grid that is regulated by STATCOM.

The outputs of both renewable sources are combined at a common DC link, which serves as the primary power bus of the system. A Static Synchronous Compensator (STATCOM) is integrated into the system to enhance voltage stability, mitigate power quality issues, and provide dynamic reactive power compensation at the point of common coupling (PCC). The STATCOM is controlled by a feedback-based controller that dynamically adjusts its operation based on voltage and current conditions to maintain system stability during transients and load fluctuations.

The consolidated DC power is fed into an AC bus through a transformer interface, which also connects the system to the utility grid and the local load. The transformer ensures proper voltage matching and galvanic isolation between the DC system and the AC grid. The controller coordinates the overall operation, including MPPT tracking, STATCOM response, and source-load balancing. This hybrid architecture enables flexible and efficient power sharing [27-28] between renewable sources, the grid, and the load, while enhancing the

Received: August 06, 2025

International Journal of Applied Mathematics
Volume 38 No. 6s, 2025
ISSN: 1311-1728 (printed version); ISSN: 1314-8060 (on-line version)

system's reliability, power quality, and grid compliance under diverse environmental and load conditions.

3 Static Synchronous Compensator (STATCOM)

STATCOM is a type of FACTS devices that uses voltage source converter (VSC) technology. It is used in energy distribution and transmission systems to offer dynamic compensation for reactive power. When connected in parallel with the B2 as shown in Figure 1, it enhances voltage regulation. It also reduces voltage stability problems caused by excessive reactive energy on the supply. VSC indirectly controls reactive energy by either producing or using it. Therefore, the criteria for achieving an improved voltage profile is accomplished. Reducing the rating for voltage helps to control VSC's cost and size, consequently transformer for coupling is required. To enhance the adaptability and robustness of STATCOM control under dynamic grid conditions, this work integrates a Whale Optimization Algorithm (WOA) to optimally tune the gains of PI controllers. The goal is to minimize voltage deviation and improve dynamic response during disturbances and load changes.

4 Whale Optimization Algorithm

Since whales are among the most intelligent animals, WOA, a new optimization technique, imitates their behaviour. Human cells share some of their brain cells. Finding the almost ideal PI control settings to regulate the flow of reactive power between the hybrid system and the STATCOM-based grid is its primary use. The STATCOM is to be driven by the PI controller. KP and KI are the two gains of the PI controller. To find the ideal PI controller parameters while minimizing J's objective function during any fault events, the WOA optimization procedure is introduced. The definition of the objective function, J, is given by Equation 1.

$$\mathbf{J} = \int_0^t (\mathbf{ev(t)^2})\mathbf{dt} \qquad (\mathbf{1})$$

In order to calculate the objective function J, which is introduced in Equation 1, the solution begins by assuming random solutions for the optimal parameters of the PI controller. WOA determines the goal function based on the updates made to the search agents at each iteration point. The optimal solution is saved after the procedure is done as many times as possible. Figure 2 shows the WOA flow chart for the best PI control parameter adjustment.

The Whale Optimization Algorithm (WOA) mimics the hunting behavior of humpback whales, particularly their bubble-net feeding strategy shown in Figure 2. This optimization process can be categorized into three primary stages: encircling prey, exploitation, and exploration.

Received: August 06, 2025

International Journal of Applied Mathematics
Volume 38 No. 6s, 2025
ISSN: 1311-1728 (printed version); ISSN: 1314-8060 (on-line version)

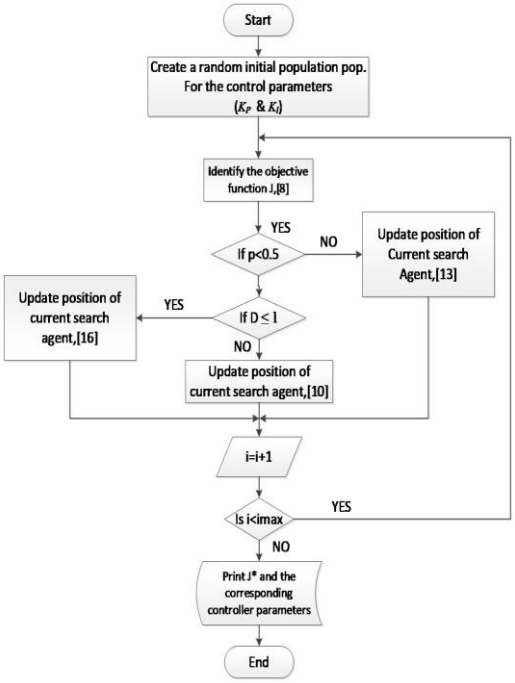

Figure 2: WOA-Based Optimization Process.

4.1 Encircling Prey (Trapping Mechanism)

Once the prey's location is identified, humpback whales instinctively swim around it in a circular motion. In the WOA context, this behavior is modeled by assuming that the best current candidate solution (referred to as the best whale) is located near the prey. Other agents in the population update their positions relative to this best solution in an attempt to converge on the global optimum. The mathematical formulation for the **encircling behavior** is given by Equation 2 & Equation 3.

$$\vec{H} = \left|\overrightarrow{E}.\overrightarrow{Y^P}(i) - \vec{Y}\,(i)\right| \tag{2}$$

$$\vec{Y}(i+1) = \overrightarrow{Y^P}\,(i) - \vec{D}\,.\overrightarrow{H} \tag{3}$$

where:

- $\vec{Y}\,(i)$is the position of the current whale at iteration iii,
- $\overrightarrow{Y^P}\,(i)$ is the position of the best solution found so far,
- $\vec{H}$ is the distance between the whale and the best solution,
- $\vec{D}$ and $\vec{E}$ are coefficient vectors.

The coefficients are calculated by Equation 4 & Equation 5.

$$\vec{E} = 2r_2 \tag{4}$$

$$\vec{D} = 2\vec{d}.r_1 - \vec{d} \tag{5}$$

where:

Received: August 06, 2025

International Journal of Applied Mathematics
Volume 38 No. 6s, 2025
ISSN: 1311-1728 (printed version); ISSN: 1314-8060 (on-line version)

- r_1 and r_2 are random numbers in the range [0, 1],
- $\vec{D}$ is a linearly decreasing parameter from 2 to 0 over the course of iterations.

This mechanism allows the whales to gradually shrink their search radius as they converge towards the optimal solution.

4.2 Exploitation Stage (Bubble-Net Attacking Method)

During the exploitation phase, the whales update their positions using two concurrent strategies: the shrinking encircling mechanism and the spiral updating position method, both of which mimic the bubble-net attack behavior.

- The **shrinking mechanism** reduces the distance between the whale and the prey by decreasing $\vec{d}$.
- The **spiral updating** simulates a helix-shaped path toward the prey.

The spiral updating is given by Equation 6.

$$\vec{Y}(i+1) = \overrightarrow{F'}.\, b_{el}(2\pi r) + \overrightarrow{Y^P}(i) \tag{6}$$

where:

- $\overrightarrow{F'}$ is the distance to the prey.
- b_{el} is a constant defining the shape of the logarithmic spiral?
- r is a random number in [0,1].

The **position update** rule combining both strategies with a 50% probability is expressed by Equation 7.

$$\vec{Y}(it+1) = \begin{cases} \overrightarrow{Y^P}\,(i) - \vec{D}.\vec{H} & p < 0.5 \\ \overrightarrow{F'}.\, b_{el}(2\pi r) + \overrightarrow{Y^P}\,(i) & p \geq 0.5 \end{cases} \tag{7}$$

where $p \in [0,1]$ is a probability factor.

4.3 Exploration Stage

In the exploration phase, whales search for new potential solutions by moving toward randomly selected whales, rather than the current best. This encourages global exploration and helps escape local optima. The equations governing the exploration behavior are given by Equation 8 & Equation 9.

$$\vec{F} = \left|\vec{D}.\overrightarrow{Y^{rand}} - \vec{Y}\right| \tag{8}$$

$$\vec{Y}(i+1) = \overrightarrow{Y^{rand}} - \vec{D}.\vec{H} \tag{9}$$

Received: August 06, 2025

International Journal of Applied Mathematics
Volume 38 No. 6s, 2025
ISSN: 1311-1728 (printed version); ISSN: 1314-8060 (on-line version)

where $\overrightarrow{Y^{rand}}$ is the position vector of a randomly chosen whale from the current population?

5 Results and Discussions

The Figure 3 represents the continuous time-wise variation of active and reactive loads on a grid-tied hybrid renewable energy system, subjected to different loading conditions categorized as Loading A, Loading B, and Loading C. These loading phases are distinctly color-shaded in the background for clarity. The system load profile is composed of four major components: LOAD-1 (2 MW, Resistive), LOAD-2 (10 MW, Resistive), LOAD-3 (8 MW, Resistive), and LOAD-4 (10 MVAR, Inductive). Each load component dynamically contributes to the total power demand at different intervals.

LOAD-1, a constant resistive load of 2 MW, remains present throughout the simulation time from 2 to 8 seconds. This base load ensures a steady-state baseline against which other transient behaviours can be evaluated. LOAD-2, representing a higher magnitude resistive load of 10 MW, is active during most of the intervals except for the Loading

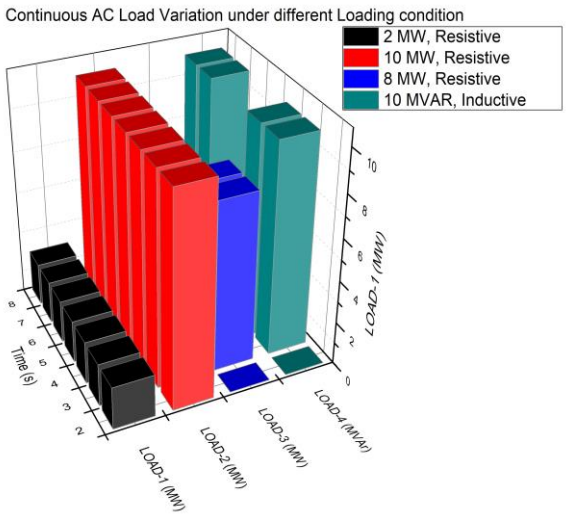

Figure 3: Continuous time-wise variation of active and reactive loads on a grid-tied hybrid renewable energy system.

C phase (5–6 seconds), where it is absent, reflecting the practical scenarios of industrial load fluctuations. LOAD-3, a mid-range resistive load of 8 MW, appears only during 3–4 seconds under the Loading B phase. It introduces a sudden surge in active power demand, simulating an abrupt load event such as motor startups or sudden industrial operations. LOAD-4, a purely reactive inductive load of 10 MVAR, is strategically activated during 3–4 seconds and again from 6.5 to 8 seconds, aligning with Loading B phases. This component introduces additional reactive power absorption, significantly stressing the system's voltage profile.

During the Loading A phases (2–3s, 4–5s, 6–7s), the system experiences moderate resistive loading conditions (12 MW), maintaining operational stability close to nominal voltage levels. In contrast, the Loading B phases (3–4s and 7–8s) are associated with significant stress due to the sudden addition of both active and reactive loads. The presence of LOAD-3 and LOAD-4 simultaneously during 3–4 seconds, and the continued presence of LOAD-4 during 6.5–8

Volume 38 No. 6s, 2025
ISSN: 1311-1728 (printed version); ISSN: 1314-8060 (on-line version)

seconds, impose severe dynamic demands on the grid, potentially causing voltage dips and transient instabilities. The brief Loading C phase (5–6s) presents a low-loading scenario with only the base load active, serving as a relief interval that tests the system's performance under light-load conditions.

From a system dynamic perspective, the interplay of high active and reactive demands during Loading B phases necessitates effective voltage regulation strategies. The Figure 3 effectively demonstrates the critical role of fast-responding devices, such as STATCOMs, to stabilize bus voltages and mitigate transient effects during these stress periods. The constructed load variation closely mimics real-world phenomena like industrial motor starting, sudden commercial load additions, and large-scale inductive load operations, thereby validating the practical relevance of the hybrid system's simulation environment.

In summary, Figure 3 provides an insightful visualization of the operational challenges encountered in hybrid renewable energy systems integrated with power grids. It offers a robust test environment for evaluating controller performance (such as WOA-PI tuned STATCOM) under diverse and practical load disturbance scenarios, thereby supporting a comprehensive performance analysis in both steady-state and dynamic conditions.

The Figure 4 presents the variation of active and reactive power at the load bus under different loading conditions. The active power (plotted in blue) fluctuates significantly over time, reflecting changes in system loading due to simulated disturbances. Notably, a sharp increase in active power is observed between 3 and 4 seconds, corresponding to a heavy load condition, followed by a sharp drop during 5 to 6 seconds representing a light load phase. Meanwhile, the reactive power (plotted in red dashed line) shows a moderate rise during high loading intervals but remains close to zero during light load conditions. This combined behaviour demonstrates the dynamic response of the hybrid system and highlights the importance of reactive power management to maintain voltage stability across varying load scenarios.

The Figure 5 presents the temporal variation of grid power under different loading conditions, specifically for Case III. Both active power and reactive power are plotted on a common Y-axis labeled Grid Power, with appropriate rescaling applied to reactive power to facilitate direct visual comparison.

The active power, represented by a blue dash-dot line, initially holds steady at approximately –2.5 MW up to 3 seconds, reflecting a stable grid supply to the connected load. Between 3 and 4 seconds, the power drops to –3.5 MW, indicating a sudden increase in load demand requiring greater power draw from the grid. Subsequently, from 4 to 5 seconds, the power level returns to –2.5 MW, suggesting a return to baseline demand. A significant change occurs from 5 to 6 seconds, where the active power sharply rises into the positive region (approximately +0.8 MW), implying a scenario of local generation exceeding demand—resulting in net power being fed into the grid. Post 6 seconds, the system stabilizes back to the initial –2.5 MW.

The reactive power, shown as a red dashed line, exhibits similar dynamic behavior

Received: August 06, 2025

International Journal of Applied Mathematics
Volume 38 No. 6s, 2025
ISSN: 1311-1728 (printed version); ISSN: 1314-8060 (on-line version)

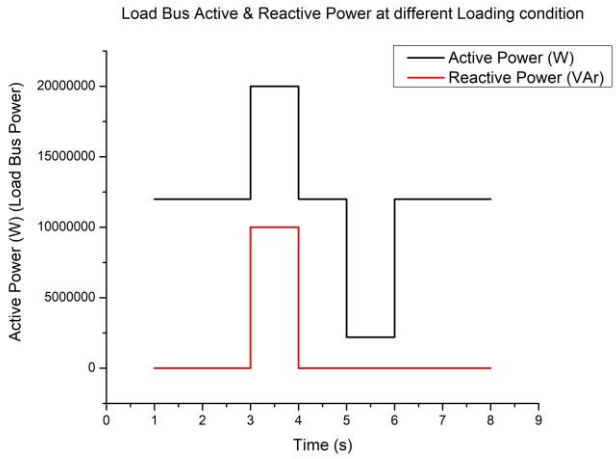

Figure 4: Active and reactive power at the load bus under different loading conditions.

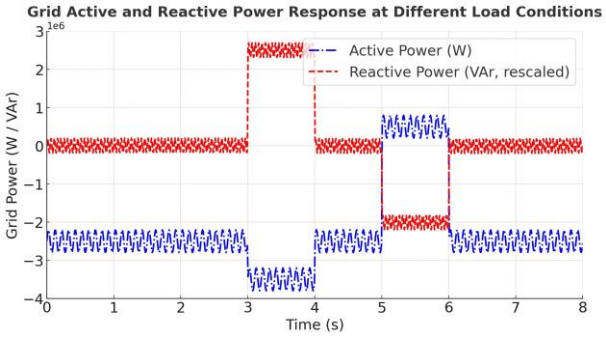

Figure 5: Temporal variation of grid power under different loading conditions.

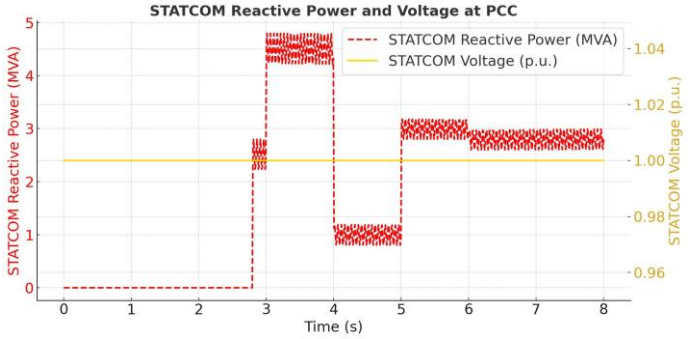

Figure 6: Real-time interaction between active and reactive power components.

with scaled values for visual alignment. It begins near zero, then rises to about 1 MVAr between 3 and 4 seconds, likely due to inductive loading. This is followed by a return to neutral reactive power levels from 4 to 5 seconds, and then a transition to negative reactive power (–1 MVAr) between 5 and 6 seconds, indicating reactive power injection, which could stem from capacitive devices or compensation strategies such as STATCOM or SVC operation. After 6 seconds, the reactive power settles back to a near-zero baseline.

Overall, the Figure 6 effectively captures the real-time interaction between active and reactive power components of a grid-connected system during varying load conditions. It reflects

International Journal of Applied Mathematics
Volume 38 No. 6s, 2025
ISSN: 1311-1728 (printed version); ISSN: 1314-8060 (on-line version)

operational scenarios such as load switching, overgeneration, and reactive power balancing, offering insights into system behavior and power quality dynamics.

Figure 6 illustrates the variation in STATCOM reactive power ($Q_{STATCOM}$) and terminal voltage ($V_{STATCOM}$) under dynamic load conditions. The red dashed line represents the reactive power output of the STATCOM, while the yellow solid line indicates the voltage at the point of common coupling (PCC).

Initially, when the system is lightly loaded (1–3 s), the STATCOM injects minimal reactive power, maintaining a voltage close to 1 pu. Between 3–4 s, as the load increases, the STATCOM compensates by injecting a higher amount of reactive power (~ 4.5 MVAR) to support voltage regulation. During the interval 4–5 s, a sudden reduction in load results in decreased reactive power output, and subsequently between 5–8 s, the STATCOM continues to modulate its output in response to varying reactive demand while maintaining voltage stability around 1 pu.

The smooth and ripple-moderated waveform of $V_{STATCOM}$ confirms the effective operation of the STATCOM in maintaining voltage regulation across fluctuating load scenarios.

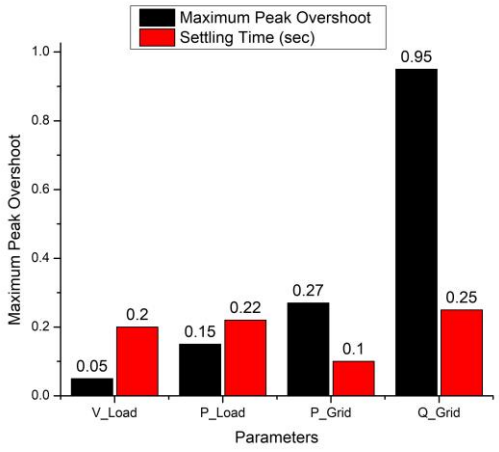

Figure 7: Performance evaluation of the proposed control strategy.

The Figure 7 illustrates the performance evaluation of the proposed control strategy in terms of maximum peak overshoot and settling time across different system parameters, namely load voltage deviation (ΔV_{Load}), load active power deviation (ΔP_{Load}), grid active power deviation (ΔP_{Grid}), and grid reactive power deviation (ΔQ_{Grid}).

In subplot (a), it is evident that the maximum peak overshoot is minimal for load voltage (ΔV_{Load}) and load active power (ΔP_{Load}), indicating effective control over local load disturbances. However, comparatively higher overshoots are observed in grid-side parameters, particularly in grid reactive power (ΔQ_{Grid}), suggesting that grid-related disturbances are more challenging to suppress completely.

Subplot (b) presents the settling time associated with these parameters. The load voltage (ΔV_{Load}) and load active power (ΔP_{Load}) demonstrate faster settling within approximately 0.2 seconds, whereas the grid reactive power (ΔQ_{Grid}) requires a relatively longer time (~ 0.25

Received: August 06, 2025

International Journal of Applied Mathematics
Volume 38 No. 6s, 2025
ISSN: 1311-1728 (printed version); ISSN: 1314-8060 (on-line version)

seconds) to stabilize. The grid active power (ΔP_{Grid}) shows the fastest settling around 0.1 seconds.

Overall, the results indicate that the control approach is highly effective in rapidly stabilizing the load-side parameters while providing reasonable damping for grid-side power deviations, thereby enhancing the dynamic stability and robustness of the hybrid system.

The provided Figure 8 & Figure 9 compare the harmonic spectra of the hybrid system's load current and load voltage under three different loading conditions: Loading-A,

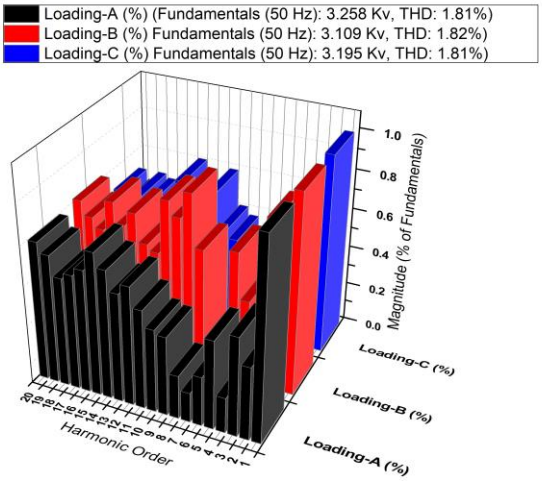

Figure 8: Harmonic spectra of the hybrid system's load voltage under three different loading conditions.

Loading-B, and Loading-C. In the first graph, representing the Load Current Harmonics Comparison, it is evident that the fundamental component (50 Hz) dominates across all loading scenarios, while higher-order harmonics are present with varying magnitudes. Loading-B exhibits relatively higher magnitudes of non-fundamental harmonics compared to Loading-A and Loading-C, indicating a higher Total Harmonic Distortion (THD) of 1.32%, as compared to 0.78% for Loading-A and 0.93% for Loading-C. This suggests that Loading-B induces more distortion in current flow, potentially stressing the power electronic interfaces.

The second graph, illustrating the Load Voltage Harmonics Comparison, similarly shows that while the fundamental (50 Hz) voltage component is predominant, there is a consistent presence of higher-order harmonics across all cases. However, the THD values for voltage remain relatively similar and low among the three loadings, with Loading-A and Loading-C each having a THD of 1.81%, and Loading-B slightly higher at 1.83%. This indicates that despite variations in load conditions, the voltage waveform quality is effectively maintained, demonstrating the robustness of the system's control strategies—particularly the STATCOM action in mitigating voltage harmonics.

Overall, while load current distortion varies more significantly across different loading scenarios, the system successfully preserves voltage waveform quality within acceptable

Received: August 06, 2025

International Journal of Applied Mathematics
Volume 38 No. 6s, 2025
ISSN: 1311-1728 (printed version); ISSN: 1314-8060 (on-line version)

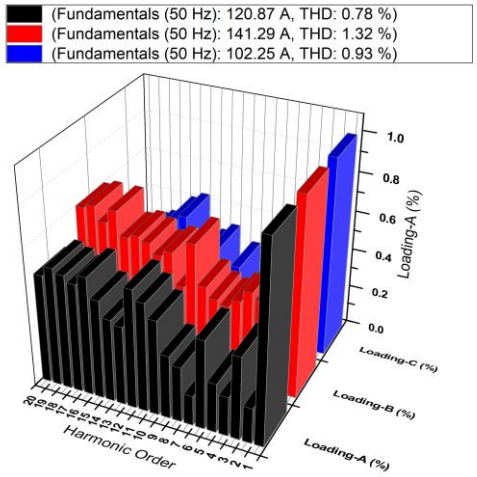

Figure 9: Harmonic spectra of the hybrid system's load current under three different loading conditions.

harmonic limits, enhancing overall power quality and system reliability.

6 Conclusion

This research investigates the effectiveness of a Whale Optimization Algorithm (WOA)tuned Proportional-Integral (PI) controlled Static Synchronous Compensator (STATCOM)—termed WOA-PI-STATCOM—deployed in a grid-connected solar-wind hybrid renewable energy system. The system is evaluated under three distinct loading scenarios developed as case studies to assess the compensator's role in improving voltage regulation, transient stability, and overall system reliability under dynamic conditions. Each case study simulates a different loading environment to emulate real-world variability. The system's performance is analyzed based on both dynamic response and transient behaviours, including voltage stability, overshoot minimization, and settling time under load disturbances. Furthermore, a quantitative assessment is conducted to compare the transient response across all scenarios, revealing that the integration of WOA-PI-STATCOM effectively maintains voltage profiles at the point of common coupling (PCC). It dynamically adjusts reactive power flow, thereby suppressing adverse effects such as over-voltages, under-voltages, and reactive power oscillations across the grid interface. The simulation results strongly support that the WOA-PI-STATCOM enhances voltage stability during varying load disturbances. By optimizing the PI controller gains using WOA, the system exhibits superior adaptability to fluctuating load demands and shows resilience against transient instabilities. Moreover, the use of WOA enables automatic tuning, ensuring optimal control action under nonlinear system dynamics without requiring manual reconfiguration. Despite its robust performance, this study deliberately focuses on idealized loading conditions, specifically uniform resistive or inductive loads, to simplify simulation complexity and emphasize core control behaviors. However, such simplified loads rarely reflect real-world electrical environments, which typically involve non-linear and unbalanced loads such as those from variable-speed motor drives, inverters, and household electronics. These practical loads introduce harmonics, current unbalance, and additional system disturbances, challenging the integrity of voltage regulation and grid stability. As an

Received: August 06, 2025

ISSN: 1311-1728 (printed version); ISSN: 1314-8060 (on-line version)

extension of this work, future research could incorporate non-linear and dynamic load profiles to better reflect practical operating conditions. Such an enhancement would provide valuable insights into the impact of real-world load characteristics on system performance and allow for a more rigorous evaluation of WOA-PI-STATCOM's capability in mitigating harmonic distortions and current imbalances. Additionally, comparative analyses involving advanced adaptive control techniques or AI-based controllers could further strengthen the findings and promote the development of more resilient and intelligent grid-integrated hybrid renewable energy systems.

7 System Description

References

[1] M. Bajaj and A. K. Sharma, "Grid integrated renewable distributed generation systems: A review of power quality challenges and mitigation techniques," Int. J. Energy Res., vol. 44, no. 6, pp. 4110–4134, 2020.

[2] Q. Zhang, Q. Hu, S. Sun, and X. Liu, "Voltage and frequency instability in large photovoltaic systems connected to weak power grids," Front. Energy Res., vol. 11, pp. 1–13, 2023.

[3] G. Rajendran et al., "A comprehensive review of solar PV integration with grid:Challenges and solutions," Energies, vol. 18, no. 9, p. 2221, 2025.

[4] A. S. Akinyemi et al., "Analysis of voltage rise phenomena in distribution systems with high renewable penetration," Sci. Rep., vol. 12, p. 8654, 2022.

[5] I. C. Barutcu et al., "Investigations on solar PV integration and power quality challenges: A case with MCS and GA," J. Electr. Appl. Sci., vol. 13, pp. 155–166, 2024.

[6] M. N. Dehaghani, "Power quality improvement in DG-based distribution systems: A review," Renew. Sustain. Energy Rev., vol. 186, p. 113857, 2025.

[7] E. Jamil, "Power quality improvement of distribution system with grid-integrated solar–wind hybrid system," Sustain. Energy Technol. Assess., vol. 36, 2019.

[8] J. K. Bhutto et al., "Adaptive controlled STATCOM and SMES for LVRT enhancement of renewable energy systems," Heliyon, vol. 11, no. 3, 2025.

[9] D. S. Ahmed and A. F. Marhoon, "STATCOM controller design for hybrid PV–wind AC microgrid," Energy Reports, vol. 10, pp. 1120–1134, 2024.

[10] S. Kumar and R. Gupta, "Performance assessment of STATCOM under variable loads using conventional and heuristic tuning," Int. J. Power Electron. Drive Syst., vol. 12, no. 3, pp. 1554–1565, 2021.

[11] P. K. Dash et al., "Reactive power control in hybrid distributed generation systems using STATCOM," IEEE Trans. Power Del., vol. 36, no. 2, pp. 1184–1195, 2021.

[12] M. Aljohani, "Enhancing performance of grid-tied renewable systems using PSO and EHO optimized controllers," Int. J. Renew. Energy Res., vol. 15, pp. 565–574, 2025.

Received: August 06, 2025

ISSN: 1311-1728 (printed version); ISSN: 1314-8060 (on-line version)

[13] N. Gupta et al., "GA-based tuning of PI controllers for voltage stability in renewable microgrids," Energy Procedia, vol. 158, pp. 2501–2506, 2022.

[14] M. Khan et al., "Differential evolution tuned STATCOM for hybrid wind–solar systems," Renew. Energy Focus, vol. 44, pp. 23–33, 2023.

[15] M. I. Mosaad, "Whale optimization algorithm-based PI controllers of STATCOM for renewable hybrid systems," World J. Model. Simul., vol. 16, no. 1, pp. 26–40, 2020.

[16] N. El Sayed et al., "Electrical grid linked to PV/wind hybrid system using fuzzy controller and STATCOM," Sci. Rep., vol. 15, p. 11830, 2025.

[17] H. B. Sharma et al., "Application of WOA in nonlinear control problems of power systems," Appl. Soft Comput., vol. 130, p. 109658, 2022.

[18] S. Rehman and F. Ahmad, "Optimized STATCOM controllers for harmonic reduction in PV-wind microgrids," Energy Convers. Manage., vol. 267, p. 116014, 2023.

[19] K. Patel and M. Singh, "Whale optimization algorithm for PI-tuned controllers in DG integrated systems," Int. J. Electr. Power Energy Syst., vol. 151, p. 109032, 2023.

[20] A. Kumar and B. Singh, "Performance enhancement of PV–PMSG hybrid renewable system using WOA-based STATCOM control," Energies, vol. 17, no. 6, p. 1555, 2024.

[21] Kumar, K., Varshney, L., Varshney, G. et al. Control strategies for energy enhancement of discontinuous GPS tracking PV system under varying weather conditions. Electr Eng (2024). https://doi.org/10.1007/s00202-023-02216-4

[22] Sampath Kumar V, Mohd. Majid, Veerendra Kumar A N, Abhinav Saxena, J.P Pandey, Amit Kumar Sharma, Kanhaiya Kumar, Palak Saxena. "Adaptive P&O Algorithm for the Controlling of Solar PV Array Based Buck Convertor". Nanotechnology Perceptions (2024): 2639-2646.

[23] Kumar, Kanhaiya, Gautam Singh, Pushpak Jain, Razia Begum, and Amit Kumar Sharma. "An Empirical Investigation into the Efficacy of Solar Panel Cooling through the Utilization of PCM." Nanotechnology Perceptions (2024): 1-9.

[24] Kanhaiya Kumar, Kumar Saurabh, Ankit Patel, Lokesh Varshney. PV Efficacy Enhancement using EHCA-MPPT by Improving Reaction Time & Power Oscillation. (2023). Leadership, Education, Personality: An Interdisciplinary Journal, ISSN: 2524-6178, 18(10), 820-830, DOI:https://doi.org/10.1366/z5nymc41.

[25] Kanhaiya Kumar, Ankit Patel, Kumar Saurabh, Lokesh Varshney. PV Panel Efficiency Enhancement using Single Ended Primary Inductor Converter under Partial Shading conditions. (2025). Leadership, Education, Personality: An Interdisciplinary

Journal, ISSN: 2524-6178, 18(11), 1013-1027, DOI: https://doi.org/10.1366/jn51rv73

[26] Kanhaiya Kumar, Lokesh Varshney, A. Ambikapathy, R. k. Saket and Mekhilef S. Solar tracker transcript—A review. Int Trans Electr Energ Syst (ITEES) .2021;31(12):e13250. doi:10.1002/2050-7038.13250.

Volume 38 No. 6s, 2025
ISSN: 1311-1728 (printed version); ISSN: 1314-8060 (on-line version)

[27] Kumar K, Varshney L, Ambikapathy, Vrinda, Sachin, Prashant, Namya. Soft Computing and IoT based Solar Tracker. International Journal of Power Electronics and Drive System (IJPEDS). Vol 12, No 3: September 2021.

[28] Kumar K, Varshney L, Ambikapathy, Inayat, Ashish, Anant, Sajal. Vision based solar tracking system for efficient energy harvesting. International Journal of Power Electronics and Drive System (IJPEDS). Vol 12, No 3: September 2021.

Received: August 06, 2025